Supporting Information for "Fault friction during simulated seismic slip pulses"

C. Harbord[1], N. Brantut [1], E. Spagnuolo [2], G. Di Toro [2,3]

[1]Department of Earth Sciences, University College London, London, UK

[2]Istituto Nazionale di Geofisica e Vulcanologia, Via di Vigna Murata 605, Rome, Italy

[3]Dipartimento di Geoscienze, Universit degli studi di Padova, Padua, Italy

Contents of this file

1. Text S1 to S3
2. Figures S1 to S5
3. Table S1

Additional Supporting Information (Files uploaded separately)

1. Caption for large Table S1
2. Captions for Movies S1 to S4

1. Text S1: Experimental reproducibility

See figure S1 for example of typical experimental reproducibility.

2. Text S2: Details of fault strength models

Temperature rise and fault strength can be estimated for our experiments by considering the coupled strength and temperature evolution for a deforming gouge layer,

$$\frac{\partial T}{\partial t} = \frac{\partial}{\partial y}\left(\alpha \frac{\partial T}{\partial y}\right) + \frac{\tau V}{\rho c W}, \tag{1}$$

where T is temperature (K), t is time (s), y is the distance perpendicular to the gouge layer m, α the thermal diffusivity (m^2s^{-1}), τ the shear stress (Pa), V the sliding velocity (m s^{-1}), ρ density (kg m^{-3}), c the heat capacity (J K^{-1}) and W the width of the shearing layer (m). Equation 1 is solved by inserting an appropriate constitutive law for τ into the above expression.

We also consider the temperature dependence of thermal conductivity, which inversely depends on temperature for a wide range of geological materials (Vosteen & Schellschmidt, 2003). For carbonate built rocks, the thermal conductivity (λ) is given by an empirically derived function of temperature after Vosteen and Schellschmidt (2003),

$$\lambda(T) = \frac{A}{B+T} + C, \tag{2}$$

where $A = 1073$, $B = 350$ and $C = 0.13$. Thermal diffusivity is considered variable in all of our numerical models, with the assumption that density and heat capacity remain constant with temperature. We note that other heat sinks may be considered in equation 1, such as de-carbonation, which is often observed during high velocity experiments at similar conditions in carbonate rock (Han et al., 2007).

Table S1. Parameters used in numerical models of strength.

Symbol	Parameter	Value	Reference
$r_{a,0}$	Initial asperity size	10 μm	-
W_{sz}	Principal slip zone width	100 μm	De Paola, Holdsworth, Viti, Collettini, and Bullock (2015); Pozzi, De Paola, Nielsen, Holdsworth, and Bowen (2018); Smith et al. (2013); Violay, Passelègue, Spagnuolo, Di Toro, and Cornelio (2019)
$W_{g,dp}$	Gouge width of De Paola et al. (2015)	1.5 mm[a]	(De Paola et al., 2015)
$W_{g,p}$	Gouge width of Pozzi et al. (2018)	1.4 mm	Pozzi et al. (2018)
$W_{g,s}$	Gouge width of Smith et al. (2013)	3 mm	Smith et al. (2013)
ρ	Density of calcite	2600 kg m^{-3}	Vosteen and Schellschmidt (2003)
c	Heat capacity of calcite	800 J K^{-1}	Vosteen and Schellschmidt (2003)
T_w	Weakening temperature	800°C	-
T_0	Ambient temperature	20°C	-
μ_0	Low velocity coefficient of friction	0.65	-
μ_w	Weakened coefficient of friction	0.05	-
$\sigma_{c,0}$	Initial indentation strength	2.75 GPa	Broz, Cook, and Whitney (2006)
N	Asperity population density	1.45x10^8 m^{-2}	Estimated at room temperature
A	Pre-exponential factor	9.55x10^4 Bar^k s$^-$1	Schmid, Boland, and Paterson (1977)
E_a	Activation enthalpy	217 kJ mol^{-1}	Schmid et al. (1977)
m	Grain size exponent	3	Schmid et al. (1977)
k	Stress exponent	1.77	Schmid et al. (1977)
α_{ss}	Thermal diffusivity of AISI 316 stainless steel	3.8x10^{-6} m^2 s^{-1}	Cverna (2002)
α_{ti}	Thermal diffusivity of Ti90Al6V4 (Grade 4 titanium)	2.26x10^{-6} m^2 s^{-1}	Cverna (2002)
α_{wc}	Thermal diffusivity of tungsten carbide	13.6x10^{-6} m^2 s^{-1}	Cverna (2002)

[a] Gouge width estimated from description of sample preparation procedure in manuscript.

2.1. Flash heating

Currently flash heating, based on the principal of localised heating at highly stressed frictional contacts, is often used to model the frictional strength and behaviour of faults in the high velocity regime (V > 0.01 m/s) (Beeler et al., 2008; Goldsby & Tullis, 2011). Rice (2006) derived a simple expression for the velocity dependant strength of a sliding surface

$$\mu = (\mu_0 - \mu_w)\frac{V}{V_w(T - T_w)} + \mu_w, \tag{3}$$

where μ_0 is the low velocity coefficient of friction (-), μ_w the weakened high velocity coefficient of friction (-), V the sliding velocity ($\mathrm{m} \cdot \mathrm{s}^{-1}$) and V_w a weakening velocity ($\mathrm{m} \cdot \mathrm{s}^{-1}$). The weakening velocity (V_w) is defined according to the physical properties of frictional contact, and defines a velocity above which asperities spend a proportion of their lifetime in a weakened state,

$$V_w(T - T_w) = \frac{\pi \alpha N_c}{r_a}\left(\frac{\rho c\,(T_w - T)}{\tau_c}\right)^2, \tag{4}$$

where r_a is the asperity length (m), T_w a weakening temperature (K), τ_c asperity shear strength (Pa) and N_c the number of contacts across the PSZ. The weakening temperature corresponds to the temperature at which some major weakening process occurs, e.g. decarbonation (Han et al., 2007) or mineral dehydration (Brantut et al., 2008).

2.2. Temperature dependant properties relevant to flash heating

In (Passelègue et al., 2014) the authours observed increases in the critical weakening velocity at elevated ambient fault temperature. This was explained by an decrease of in indentation strength with temperature (Evans & Goetze, 1979), reasoning that the

reduced heat generation at asperities lead to an increased critical weakening velocity. Evans and Goetze (1979) demonstrated in experiments that the indentation strength (σ_c) of crystalline geological materials has an inverse temperature dependance, where strength is given by

$$\sigma_c = \sigma_0 T^{-\frac{1}{n}}, \tag{5}$$

where σ_0 is a prefactor (Pa k^n) and n an asperity stress exponent. For olivine polycrystals Evans and Goetze (1979) found $n = 2$. Here we consider changes in asperity strength with temperature, and in the absence of temperature dependant indentation strength measurements of calcite we define an equation of the form:

$$\sigma_c(T) = \sigma_{c,0} \left[\frac{T}{T_w - T_0} \right]^{-1/n}, \tag{6}$$

where $\sigma_{c,0}$ asperity strength at T=20°C. The exponent, n can be considered analogous to a stress exponent, reflecting the plastic nature of asperity contact.

Given that the real area of contact A_r is given by the ratio of normal stress to indentation strength, we may also expect a change in asperity size with temperature. To define a function for the temperature dependence of asperity size we consider that for a given indentation strength and temperature, the number of asperities per unit surface area is

$$N = \kappa \frac{\sigma_c}{\sigma_n} r_a^{-2}, \tag{7}$$

where κ is a shape factor ($= \frac{4}{\pi}$ for circular asperities, or $= 1$ for square asperities). If we make the assumption that the number of asperities per unit fault area remains constant with temperature, then the temperature dependence of asperity size is

$$r_a(T) = \sqrt{\frac{\sigma_n}{N \kappa \sigma_c(T)}}, \tag{8}$$

where N is the number of asperities per unit area evaluated at T=20°C.

2.3. Grain size sensitive creep

In carbonate built faults the common post-mortem observation of nanometric grains, combined with the expectation high fault temperatures during rapid deformation has led a number of authors to suggest that grain size sensitive creep accommodates fault weakening at high velocity (De Paola et al., 2015; Pozzi et al., 2018; Violay et al., 2019). For a model of plastic creep governing fault strength we adopt the following constitutive relationship derived by Schmid et al. (1977)

$$\tau = \left[\dot{\gamma} d^{-m} A e^{-\frac{E_a}{RT}}\right]^k, \tag{9}$$

where d is the grain size (m), m a grain size exponent (-), $\dot{\gamma} = V(t)/W$ the shear strain rate (s^{-1}), A a pre-exponential factor ($Bar^{-k}s^{-1}$), E_a the activation enthalpy (kJ Mol^{-1}), R the gas constant (J K^{-1} mol^{-1}) and k a stress exponent (-).

2.4. Model geometry

Equation 1 is solved in non dimensional form by applying the transform,

$$\begin{aligned} \tilde{y} &= \tfrac{y}{W} \\ \tilde{t} &= \tfrac{t\alpha_0}{W^2} \\ \tilde{T} &= \tfrac{T-T_0}{T_w-T_0}, \end{aligned} \tag{10}$$

with T_w set according to the values in table S1 for both fault rheologies. We solved 1 using a method of lines, centred in space and forward in time, with thermal diffusivity centrally averaged across nodes according the ambient temperature.

2.4.1. Model geometry with cohesive annular samples

In the simple case of initially bare surface experiments, we used a half space model comprising a slip zone of thickness W_{sz}, where y is normalised by the principle slip zone width (figure S2). Thermal and physical properties are the same across the model domain. Ten linearly spaced nodes were used to define the principle slip zone, outside of this, logarithmic spacing was used within the 'wall rock', with the total model set according to the characteristic diffusion length $L = t_{max}/(\alpha_0/W_{sz}^2)$. We used a symmetric model, and at $\tilde{y} = L$ a constant temperature was imposed,

$$\left.\frac{\partial \tilde{T}}{\partial \tilde{t}}\right|_L = 0 \tag{11}$$

2.4.2. Gouge models

For models involving a gouge layer and sample holders we seperated the model into 4 domains (figure S3): bottom sample holder, with appropriate metal thermal conductivities as defined in the main text (stationary side in De Paola et al. (2015) and Pozzi et al. (2018), rotary side in Smith et al. (2013)), 2) inactive gouge layer with the same thermal and physical properties as the PSZ, 3) the PSZ accomodating all deformation evenly across the layer, 4) top gouge holder (rotary side in De Paola et al. (2015) and Pozzi et al. (2018), stationary side in Smith et al. (2013)). A constant temperature was imposed at the model boundaries, $[|-\tilde{y}|, +\tilde{y}] = L \gg W$:-

$$\left.\frac{\partial \tilde{T}}{\partial \tilde{t}}\right|_{-L,+L} = 0 \tag{12}$$

2.5. Numerical model benchmark

In order to test the reliability of our numerical models we performed two benchmarks of our code for an adiabatic case (no off-fault heat diffusion) and a slip on a plane solution using the closed from asymptotic solutions given by Brantut and Viesca (2017). The adiabatic solution was computed by setting off-fault thermal diffusivity equal to zero (figure S4). To approximate a semi-infinite half space relevant to the case of slip on a plane we used $L \approx 10^8 W_{psz}$, and ran the solution to large timescales to check solution convergance (see figure S5).

3. Text S3: Elastodynamic models

In order to asses the compatibility of our experimental data with elastodynamic equilibrium we solved for a slip pulse propagating at constant rupture velocity with constant source duration. In this case elastodynamic equilibrium is satisfied when,

$$\tau(x) = \tau_b + \frac{G^*}{2\pi V_r} \int_0^L \frac{V(s)}{s-x} ds, \tag{13}$$

where $\tau(x)$ is the elastic stress, τ_b is the ambient fault traction, $G^* = S\sqrt{1 - V_r/C_s}$ is the modified shear modulus and $L = V_r t_r$ the rupture length. By non-dimensionalising and transforming $2x/L - 1 \rightarrow x$, $(\tau - \tau_b)/\tau_0 \rightarrow \tau$ and $V/(\tau_0 V_r/G^*) \rightarrow V$ then equation 13 becomes

$$\tau(x) = \tau_b + \frac{1}{\pi} \int_{-1}^{1} \frac{V(s)}{s-x} ds. \tag{14}$$

When using the imposed velocity history as a boundary condition, we calculated elastic stress using a Gauss-Chebyshev quadrature (see Viesca and Garagash (2018) for a detailed description of these techniques). Stress was computed using 501 nodes based on the input velocity history.

When solving the slip pulse model using the experimentally measured traction evolution we first applied a 1000 point moving average window to the data to smooth the model input. We then solved equation 13 for velocity using again a Gauss-Chebyshev quadrature approximation with 501 nodes. By imposing the additional conditions $V(0) = 0$ and $V(L) = 0$, a solution for τ_b is also determined.

4. User uploaded files

Large table S1 Inventory of experiments and associated parameters.

Movie S1. Video of experiment S1765f, Carrara Marble, $t_s = 0.075$ s.

Movie S2. Video of experiment S1764c, Carrara Marble, $t_s = 0.4$ s.

Movie S3. Video of experiment S1762d, Etna Basalt, $t_s = 0.3$ s.

Movie S4. Video of experiment S1752h, Etna Basalt, $t_s = 0.6$ s.

References

Beeler, N. M., Tullis, T. E., & Goldsby, D. L. (2008). Constitutive relationships and physical basis of fault strength due to flash heating. *J. Geophys. Res. Solid Earth*, *113*(1), 1–12. doi: 10.1029/2007JB004988

Brantut, N., & Platt, J. D. (2017). Dynamic Weakening and the Depth Dependence of Earthquake Faulting. , 171–194. Retrieved from `http://doi.wiley.com/10.1002/9781119156895.ch9` doi: 10.1002/9781119156895.ch9

Brantut, N., Schubnel, A., Rouzaud, J. N., Brunet, F., & Shimamoto, T. (2008). High-velocity frictional properties of a clay-bearing fault gouge and implications for earthquake mechanics. *J. Geophys. Res. Solid Earth*, *113*(10), 1–18. doi: 10.1029/2007JB005551

Brantut, N., & Viesca, R. C. (2017). The fracture energy of ruptures driven by flash heating. *Geophys. Res. Lett.*, *44*(13), 6718–6725. doi: 10.1002/2017GL074110

Broz, M. E., Cook, R. F., & Whitney, D. L. (2006). Microhardness, toughness, and modulus of Mohs scale minerals. *Am. Mineral.*, *91*(1), 135–142. doi: 10.2138/am.2006.1844

Cverna, F. (2002). *ASM Ready Reference: Thermal Properties of Metals*. ASM International. Retrieved from `https://app.knovel.com/hotlink/toc/id:kpASMRRTP1/asm-ready-reference-thermal/asm-ready-reference-thermal`

De Paola, N., Holdsworth, R., Viti, C., Collettini, C., & Bullock, R. J. (2015). Can grain size sensitive flow lubricate faults during the initial stages of earthquake propagation? *Earth Planet. Sci. Lett.*, *431*, 48–58. Retrieved from `http://dx.doi.org/10.1016/j.worlddev.2005.07.015{\%}5Cnhttp://`

scitation.aip.org/content/aip/journal/jap/102/2/10.1063/1.2756072 doi: 10.1063/1.2756072

Evans, B., & Goetze, C. (1979). The temperature variation of hardness of olivine and its implication for polycrystalline yield stress. *J. Geophys. Res.*, *84*(B10), 5505–5524. doi: 10.1029/JB084iB10p05505

Goldsby, D. L., & Tullis, T. E. (2011, oct). Flash Heating Leads to Low Frictional Strength of Crustal Rocks at Earthquake Slip Rates. *Science (80-.).*, *334*(6053), 216–218. Retrieved from https://www.sciencemag.org/lookup/doi/10.1126/science.1207902 doi: 10.1126/science.1207902

Han, R., Shimamoto, T., Hirose, T., Ree, J.-H., & Ando, J.-i. (2007, may). Ultralow Friction of Carbonate Faults Caused by Thermal Decomposition. *Science (80-.).*, *316*(5826), 878–881. Retrieved from http://www.sciencemag.org/cgi/doi/10.1126/science.1139763 doi: 10.1126/science.1139763

Passelègue, F. X., Goldsby, D. L., & Fabbri, O. (2014, feb). The influence of ambient fault temperature on flash-heating phenomena. *Geophys. Res. Lett.*, *41*(3), 828–835. Retrieved from http://doi.wiley.com/10.1002/2013GL058374 doi: 10.1002/2013GL058374

Pozzi, G., De Paola, N., Nielsen, S. B., Holdsworth, R. E., & Bowen, L. (2018). A new interpretation for the nature and significance of mirror-like surfaces in experimental carbonate-hosted seismic faults. *Geology*, *46*(7), 583–586. doi: 10.1130/G40197.1

Rice, J. R. (2006). Heating and weakening of faults during earthquake slip. *J. Geophys. Res. Solid Earth*, *111*(5), 1–29. doi: 10.1029/2005JB004006

Schmid, S. M., Boland, J. N., & Paterson, M. S. (1977). Superplastic flow in finegrained

limestone. *Tectonophysics*, *43*(3-4), 257–291. doi: 10.1016/0040-1951(77)90120-2

Smith, S. A., Di Toro, G., Kim, S., Ree, J. H., Nielsen, S., Billi, A., & Spiess, R. (2013). Coseismic recrystallization during shallow earthquake slip. *Geology*, *41*(1), 63–66. doi: 10.1130/G33588.1

Viesca, R. C., & Garagash, D. I. (2018). Numerical Methods for Coupled fracture problems. *J. Mech. Phys. Solids*, *113*, 13–34. doi: 10.1016/j.jmps.2018.01.008

Violay, M., Passelègue, F. X., Spagnuolo, E., Di Toro, G., & Cornelio, C. (2019). Effect of water and rock composition on re-strengthening of cohesive faults during the deceleration phase of seismic slip pulses. *Earth Planet. Sci. Lett.*.

Vosteen, H. D., & Schellschmidt, R. (2003). Influence of temperature on thermal conductivity, thermal capacity and thermal diffusivity for different types of rock. *Phys. Chem. Earth*, *28*(9-11), 499–509. doi: 10.1016/S1474-7065(03)00069-X

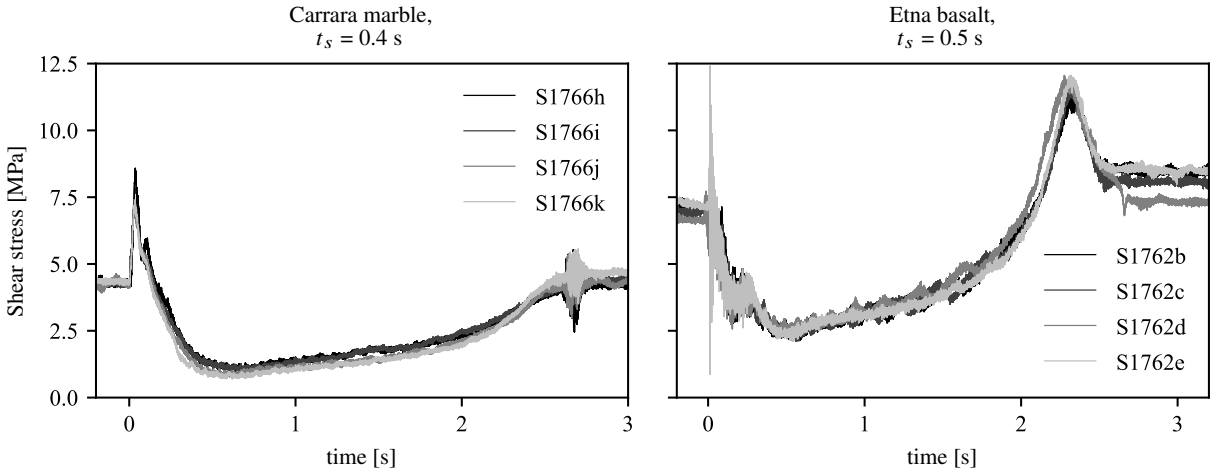

Figure S1. Example of test reproducibility

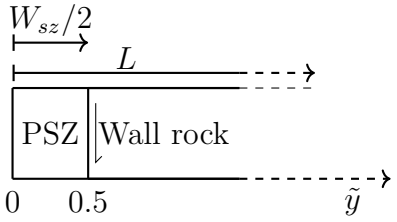

Figure S2. Bare surface model geometry

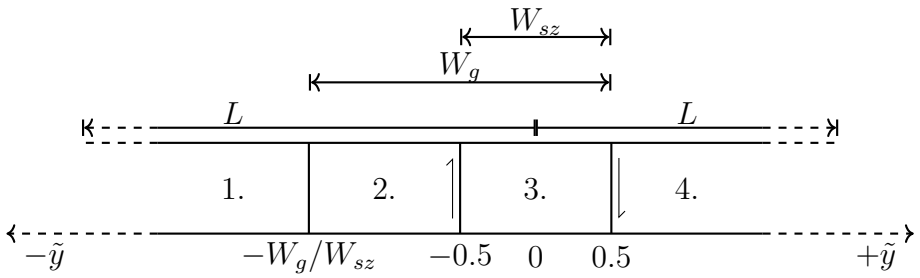

Figure S3. Gouge model geometry, 1. and 4. = metal gouge holder, 2. inactive gouge layer, 3. principal slip zone

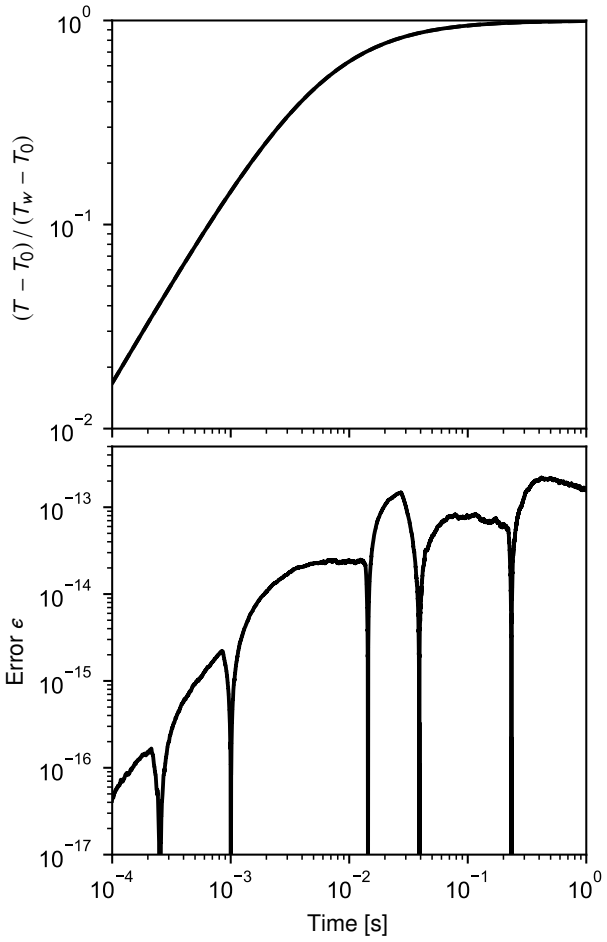

Figure S4. Benchmark of numerical code against closed form solution from Brantut and Platt (2017) for an adiabatic flash heating case where off-fault thermal diffusion is neglected.

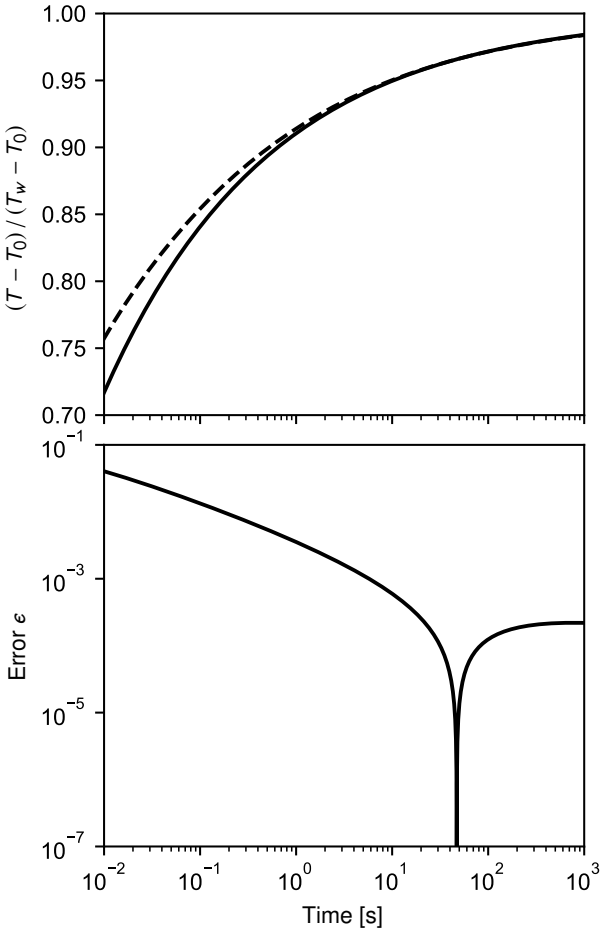

Figure S5. Benchmark of numerical code (dashed curve) against the closed form solution (solid curve) from Brantut and Platt (2017) for a slip on a plane flash heating case.

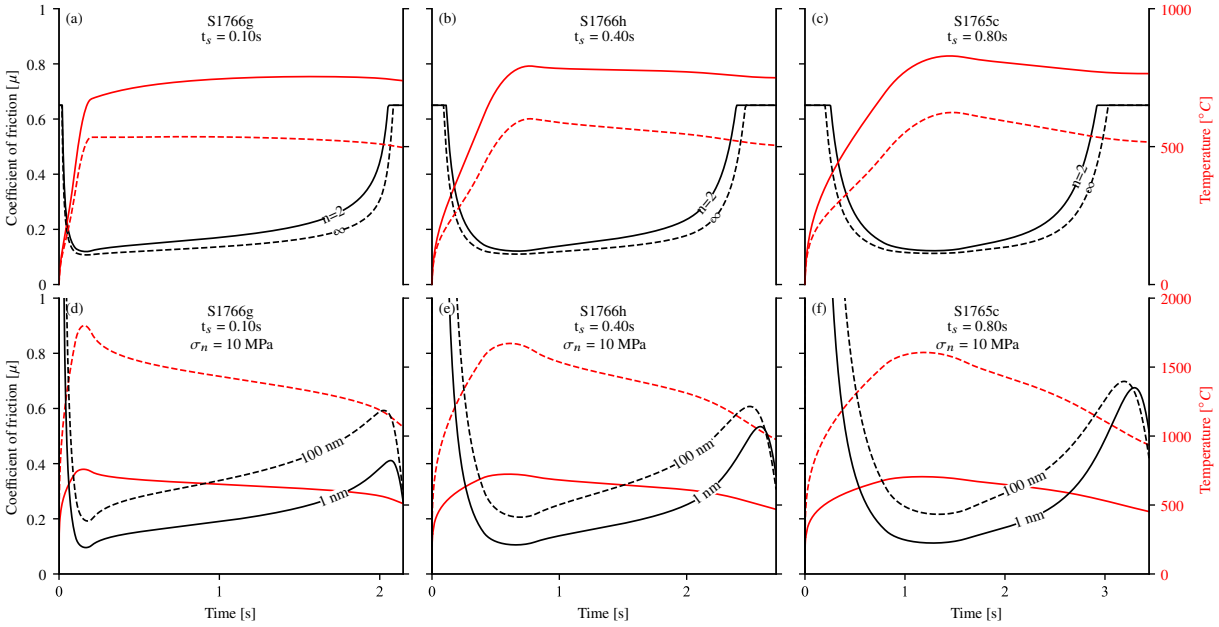

Figure S6. Modelled temperature for presented experiments. Insets a)-c) are flash heating models and d)-f) are GSS creep models, red curves are temperature and black curves the modelled strength.